A Fc-free EGFR-specific 4-1BB-agonistic trimerbody displays non-toxic broad anti-tumor activity in humanized murine cancer models

Marta Compte[1], Sean deán L. Harwood[2], Ainhoa Erce-Llamazares[1,3,4], Antonio Tapia-Galisteo[5], Eduardo Romero[6], Irene Ferrer[7,8], Eva M. Garrido-Martin[7,8#], Ana B. Enguita[9,10], Maria C. Ochoa[11], Belén Blanco[3,4], Marta Oteo[6], Nekane Merino[12], Daniel Nehme-Álvarez[3,4], Oana Hangiu[3,4], Carmen Domínguez-Alonso[3,4], Manuela Zonca[1], Angel Ramírez-Fernández[3,4], Francisco J. Blanco[13], Miguel A. Morcillo[6], Ines G. Muñoz[14], Ignacio Melero[11,8,15,16], José L. Rodriguez-Peralto[8,9,10,17], Luis Paz-Ares[7,8,18,19], Laura Sanz[5], Luis Alvarez-Vallina[2,3,4*]

[1]Department of Antibody Engineering, Leadartis SL, 28008 Madrid, Spain; [2]Immunotherapy and Cell Engineering Laboratory, Department of Engineering, Aarhus University, 8000 C Aarhus, Denmark; [3]Cancer Immunotherapy Unit (UNICA), Department of Immunology, Hospital 12 de Octubre, 28041 Madrid, Spain; [4]Immuno-Oncology and Immunotherapy Group, Instituto de Investigación Sanitaria 12 de Octubre (imas12), 28041 Madrid, Spain; [5]Molecular Immunology Unit, Hospital Universitario Puerta de Hierro Majadahonda, 2822 Majadahonda, Madrid, Spain; [6]Biomedical Applications and Pharmacokinetics Unit, Centro de investigaciones Energéticas, Medioambientales y Tecnológicas (CIEMAT), 28040 Madrid, Spain; [7]H12O-CNIO Lung Cancer Clinical Research Unit, Instituto de Investigación Sanitaria 12 de Octubre (imas12), and Centro Nacional de Investigaciones Oncológicas (CNIO), 28041 Madrid, Spain; [8]Centro de Investigación Biomédica en Red en Oncología (CIBERONC), Madrid, Spain; [9]Department of Pathology, Hospital Universitario 12 de Octubre, 28041 Madrid, Spain; [10]Department of Pathology. Universidad Complutense, 28040 Madrid, Spain; [11]Department of Immunology and Immunotherapy, Center for Applied Medical Research (CIMA), University of Navarra, Pamplona, Spain; [12]Structural Biology Unit, CIC bioGUNE, Parque Tecnológico de Bizkaia, 48160 Derio, Spain; [13]Structural and Chemical Biology Department, Centro de Investigaciones Biológicas, CIB-CSIC, Madrid, 28040, Spain; [14]Crystallography and Protein Engineering Unit, Structural Biology Programme, Centro Nacional de Investigaciones Oncológicas (CNIO), 28029 Madrid, Spain; [15]Department of Immunology, University Clinic, University of Navarra, Pamplona, Spain; [16]Instituto de Investigación Sanitaria de Navarra (IdISNA), Pamplona, Spain; [17]Cutaneous Oncology Group, Instituto de

Investigación Sanitaria 12 de Octubre (imas12), 28041 Madrid, Spain; [18]Department of Medical Oncology, Hospital Universitario 12 de Octubre, 28041 Madrid, Spain; [19]Department of Medicine. Universidad Complutense, 28040 Madrid, Spain.

Running title: Non-toxic broad anti-tumor activity of an EGFR×4-1BB bispecific trimerbody

Keywords: 4-1BB, bispecific antibody, trimerbody, checkpoint blockade, PD-L1, T cells

* Corresponding author:
Luis Alvarez-Vallina.
Tel.: +34 917792773
Email: lav.imas12@h12o.es

[#]Current address: Department of Cell Biology and Pharmacogenomics. PharmaMar S.A. 28770 Colmenar Viejo, Madrid. Spain.

Conflict of interest disclosure statement

MC, AE-L and MZ are current or former employees of Leadartis. LS and L.A-V. are co-founders of Leadartis. The remaining authors declare no competing interests.

Word count: 5072
Figures: 4

Funding

Research was supported by grants from the European Union [IACT Project (602262), H2020-iNEXT (1676)]; the Spanish Ministry of Science, Innovation and Universities and the Spanish Ministry of Economy and Competitiveness (SAF2017-89437-P, CTQ2017-83810-R, RTC-2016-5118-1, RTC-2017-5944-1), partially supported by the European Regional Development Fund; the Carlos III Health Institute (PI16/00357), co-founded by the Plan Nacional de Investigación and the European Union; the CRIS Cancer Foundation (FCRIS-IFI-2018); and the Spanish Association Against Cancer (AECC, 19084). LR-P was supported by a predoctoral fellowship from the Immunology Chair, Universidad Francisco de Vitoria/Merck. CD-A was supported by a predoctoral fellowship from the Spanish Ministry of Science, Innovation and Universities (PRE2018-083445). MZ was supported by the Torres Quevedo Program from the Spanish Ministry of Economy and Competitiveness, co-founded by the European Social Fund (PTQ-16-08340).

TRANSLATIONAL RELEVANCE

Despite their efficacy in preclinical studies, full-length 4-1BB-agonistic IgGs have not advanced in clinical development due to their severe hepatotoxicity. In this study, we provide preclinical proof-of-concept for a humanized Fc-free tumor-specific 4-1BB-agonistic trimerbody demonstrating anti-tumor activity against a wide range of human tumors in humanized immunoavatar mice, as well as synergy with immune checkpoint blockers. This approach which may provide a way to elicit responses in most cancer patients while avoiding Fc-mediated adverse reactions. These findings demonstrate that EGFR is an effective target for the development of a broadly applicable tumor-specific 4-1BB mediated immunotherapy, and support the development of the Trimerbody®-EGFR×4-1BB as a clinical candidate for treatment of advanced solid tumors.

ABSTRACT

Background The induction of 4-1BB signaling by agonistic antibodies can drive the activation and proliferation of effector T cells and thereby enhance a T cell-mediated anti-tumor response. Systemic administration of anti-4-1BB-agonistic IgGs, although effective preclinically, has not advanced in clinical development due to their severe hepatotoxicity.

Methods Here, we generated a humanized EGFR-specific 4-1BB-agonistic trimerbody, which replaces the IgG Fc region with a human collagen homotrimerization domain. It was characterized by structural analysis and *in vitro* functional studies. We also assessed pharmacokinetics, anti-tumor efficacy, and toxicity *in vivo*.

Results In the presence of a T cell receptor signal, the trimerbody provided potent T cell costimulation that was strictly dependent on 4-1BB hyperclustering at the point of contact with a tumor antigen-displaying cell surface. It exhibits significant anti-tumor activity *in vivo*, without hepatotoxicity, in a wide range of human tumors including colorectal and breast cancer cell-derived xenografts, and non-small-cell lung cancer patient-derived xenografts associated with increased tumor-infiltrating $CD8^+$ T cells. The combination of the trimerbody with a PD-L1-blocker led to increased IFNγ secretion *in vitro* and resulted in tumor regression in humanized mice bearing aggressive triple-negative breast cancer.

Conclusions These results demonstrate the non-toxic broad anti-tumor activity of humanized Fc-free tumor-specific 4-1BB-agonistic trimerbodies and their synergy with checkpoint blockers, which may provide a way to elicit responses in most cancer patients while avoiding Fc-mediated adverse reactions.

INTRODUCTION

Modulating immune responses using monoclonal antibodies (mAbs) is one of the most promising approaches for cancer immunotherapy (1). Probably most well-known is the mAb-mediated blockade of the programmed cell death protein 1 (PD-1) inhibitory pathway, which prevents PD-1-mediated immunosuppressive signaling in T cells and can restore effector functions to anergic tumor-infiltrating T cells (2). PD-1/PD-ligand 1 (PD-L1) axis blockade has shown long-term durable responses in a wide range of cancers, but their efficacy is limited to 10-30% of patients (3). Another immunotherapeutic approach involves the stimulation of costimulatory receptors, such as 4-1BB, with agonistic mAbs (4). 4-1BB, also known as CD137, is a member of the TNF receptor (TNFR) superfamily which can be induced on a variety of leukocyte subsets. 4-1BB is a type I single-pass transmembrane receptor with four extracellular cysteine-rich domains (CRDs) and an intracellular signaling domain (5). On T cells, 4-1BB is expressed following activation through the T cell receptor (TCR). Binding of its natural ligand [4-1BB-Ligand (4-1BBL), TNFSF9] or agonistic mAbs enhances T cell proliferation and effector functions (6-8), prevents T cell exhaustion (8), protects from programmed cell death (9, 10), and promotes memory cell differentiation, which may support persistence of tumor-specific T cells (11). Anti-4-1BB-agonistic mAbs have been explored in preclinical cancer models and shown to promote rejection of a range of poorly immunogenic tumors (12-14). However, off-tumor toxicity have been the major impediment to the clinical development of full-length anti-human 4-1BB (anti-hu4-1BB)-agonistic IgGs, and several studies suggest that the toxicity is mainly dependent on Fc-FcγR interactions (15-17). The anti-hu4-1BB human IgG_4 urelumab (BMS-663513) caused dose-dependent liver toxicity and was implicated in two deaths (18, 19). Subsequent studies revealed that lower doses reduced liver toxicity, but at the cost of efficacy (19). The anti-hu4-1BB human IgG_2 utomilumab (PF-05082566) has an improved safety profile relative to urelumab, but is also a less potent 4-1BB agonist (20).

New strategies are being actively sought to avoid the off-tumor toxicities associated with Fc-FcγR interactions while retaining the anti-tumor activity associated with 4-1BB costimulation. These approaches aim to confine 4-1BB costimulation to the tumor microenvironment and draining lymph nodes. We have recently described Fc-free tumor-specific trimerbodies targeting a tumor-associated antigen (TAA), such as EGFR

(epidermal growth factor receptor) (15) or CEA (carcinoembryonic antigen)(21), and murine 4-1BB in an agonistic manner. Both trimerbodies were potent costimulators *in vitro* and the EGFR-targeted 4-1BB-agonistic trimerbody showed enhanced tumor penetration and powerful anti-tumor activity in immunocompetent mice, while alleviating the systemic cytokine production and T cell-mediated liver toxicities that are associated with IgG-based 4-1BB agonists (15). More recently, we showed in a liver-specific human EGFR-transgenic immunocompetent mouse that systemic administration of anti-4-1BB-agonistic IgGs resulted in nonspecific immune stimulation and hepatotoxicity, whereas in mice treated with the Fc-free EGFR-specific 4-1BB-agonistic trimerbody no such immune-related adverse effects were observed (22).

Here, we generated and characterized a humanized EGFR-targeted 4-1BB-agonistic trimerbody (4-1BB$^{N/C}$EGFR), consisting of three anti-hu4-1BB single-chain antibody fragments (scFv) and three anti-human EGFR (huEGFR) single-domain antibodies (V_{HH}). The humanized 4-1BB$^{N/C}$EGFR is structurally similar to that of the mouse trimerbody (15), costimulates human T cells *in vitro* in the presence of huEGFR, and delayed the progression of an EGFR^{+} human colorectal cancer (CRC) and triple-negative breast cancer (TNBC) cell line-derived xenografts (CLDX) and a patient-derived xenograft (PDX) of EGFR^{+} non-small-cell lung cancer (NSCLC), as monotherapy in immune-reconstituted mice. Furthermore, the combination of 4-1BB$^{N/C}$EGFR with the immune checkpoint blocker (ICB) atezolizumab significantly improved the anti-tumor immune response, with a near-complete inhibition of tumor growth in humanized mice bearing aggressive EGFR^{+} PD-L1^{+} human TNBC CLDX.

MATERIAL AND METHODS

Mice

NOD.Cg-Prkdc^{SCID}IL2rg^{tm1Wjl}/SzJ (NSG) female mice were supplied by Charles River, Hsd:athymic Nude-Foxn1^{nu} female mice were supplied by Envigo RMS SPAIN S.L., and 129S4-Rag2tm1.1Flv Il2rgtm1.1Flv/J (Rag2 -/- IL2Rγ null) female mice were bred in the animal facility of CIMA. Animals were maintained under specific-pathogen-free condition with daily cycles of 12 hours light / 12 hours darkness, and sterilized water and food were available ad libitum. All animal procedures conformed to European Union Directive 86/609/EEC and Recommendation 2007/526/EC, enforced in Spanish law under RD 1201/2005. Animal protocols were approved by the respective Ethics Committee of Animal Experimentation of the participant institutions (IDIPHISA,

imas12, CIEMAT and CIMA); they were performed in strict adherence to the guidelines stated in the International Guiding Principles for Biomedical Research Involving Animals, established by the Council for International Organizations of Medical Sciences (CIOMS). The experimental study protocols were additionally approved by local government (PROEX 094/15, 108/15, 076/19 and 166/19).

Antibodies and cell lines

Commercially available antibodies used in the experiments are listed in Table S1. Recombinantly produced antibodies are listed in a Table S2. HEK293 (CRL-1573), MDA-MB-231 (HTB-26), A431 (CRL-1555), NIH/3T3 (CRL-1658) and CHO-K1 (CCL-61) cells were obtained from the American Type Culture Collection and cultured in Dulbecco's modified Eagle's medium (DMEM) (Lonza) supplemented with 2 mM L-glutamine, 10% (vol/vol) heat inactivated Fetal Calf Serum (FCS) (Merck Life Science), and antibiotics (100 units/mL penicillin, 100 mg/mL streptomycin) (all from Life Technologies) referred as to DMEM complete medium (DCM), at 37 ºC in 5% CO_2 humidity. NIH/3T3 cells expressing huEGFR ($3T3^{huEGFR}$) (23) were kindly provided by Dr A. Villalobo (IIBm, Madrid, Spain). The hu4-1BB-expressing HEK293 cell line ($HEK239^{hu4\text{-}1BB}$) was generated by transfection with the expression vector pCMV3-Flag-TNFRSF9 (SinoBiological) and selected in DCM with 500 µg/mL G418 (Life Technologies). CHO-K1 Cells expressing human FcγRIIb (CD32) were from Promega (#JA2251). The cell lines were routinely screened for the absence of mycoplasma contamination by PCR using the Mycoplasma Plus TM Primer Set (Biotools B&M Labs).

Construction of expression vectors

To generate the SAP3.28 scFv-based N-terminal trimerbody, the DNA fragments encoding the FLAG-strep II-$SAP3.28^{HL}$ (V_H-linker-V_L) scFv was synthesized by Geneart AG and subcloned as *Hind*III/*Not*I into the expression vector $pCR3.1\text{-}MFE23^{N}$ (24) resulting in pCR3.1-FLAG-strepII-$SAP3.28^{HL\text{-}N}$-myc/His. The C-terminal myc/His tag-sequence was removed by PCR from the plasmids with Fw-CMV and Stop-*Xba*I-Rev primers (Table S3). The Flag-strep II-$SAP3.28^{HL}$ scFv gene was subcloned as *Hind*III/*Not*I into a vector containing the human collagen XVIII-derived homotrimerization (TIE^{XVIII}) domain and the anti-human EGFR single-domain antibody (V_{HH}; EGa1) (25), resulting in the bispecific trimerbody-expressing vector pCR3.1-

FLAG-strepII-SAP3.28$^{HL\text{-}N18/C18}$EGa1. All the sequences were verified using primers FwCMV and RvBGH (Table S3).

In vitro 4-1BB-dependent NF-κB activation assay

4-1BB-dependent activation of activated nuclear factor kappa-B (NF-κB) assay was performed on thaw-and-use (T&U) GloResponse^{TM}NFkB-*luc2*/4-1BB Jurkat cells (Promega, #JA2351) according to the manufacturer's instructions (Supplementary Methods).

Human PBMC and T cells activation assays

Human PBMCs or isolated T cells (Supplementary Methods) (1.5 x 10^5 cells/well) were plated in triplicate in flat bottom 96-well plates, in RPMI supplemented with 10% FCS and 50 µM β-mercaptoethanol (Life Technologies) and co-cultured with 45 Gy irradiated target cells (3T3 or 3T3^{hEGFR}) at an effector/target ratio of 5:1. The anti-hu4-1BB agonists antibodies and controls were added at ten-fold serial dilutions in the presence of anti-huCD3 (OKT3) mAb at 0.05 µg/ml. After 72 hours, cell-free supernatants were analyzed by ELISA for cytokine secretion. Irradiated EGFR$^+$PD-L1$^-$ cells (3T3^{huEGFR}) or EGFR$^+$PD-L1$^+$ cells (MDA-MB-231) (3 x 10^4 cells/well) were seeded with huPBMCs (1.5 x 10^5 cells/well), activated with anti-huCD3 at 0.05 µg/ml, in the presence of anti-PD-L1 (atezolizumab) alone (10 µg/ml) or combined with 4-1BB$^{N/C}$EGFR (1 µg/ml). Cell-free supernatants were measured for IFNγ after 72 hours by ELISA (Diaclone, #851560005).

Humanized colorectal cancer cell line-derived xenograft (CDLX) models

HT29 cells (1 x 10^6), were implanted s.c. into the dorsal space of 6-week-old Rag2 -/- IL2Rγ null female mice, followed by the i.p. infusion of freshly huPBMCs (1 x 10^7 cells/mouse). Tumor growth was monitored by caliper measurements three times a week, and when tumors reached approximately 0.4 cm in diameter, mice were randomized to receive treatment (n = 7-8/group). Measurements were conducted in a random order by the investigator who was blinded to the treatment assignment. Mice were treated every three days with five i.p. injections of CEA^N or 4-1BB$^{N/C}$EGFR trimerbodies (4 mg/kg) or every week with three i.p. injections of 4-1BB IgG (4 mg/kg). MDA-MB-231cells (2 x 10^6), were resuspended in PBS and mixed with matrigel (30%). Cells were implanted s.c. on right dorsal flank of 6-week-old NSG

female mice, followed by an i.p. injection of freshly isolated huPBMCs (1 x 10^7cells/mouse). Tumor growth was monitored by caliper measurements three times a week. Tumor-bearing mice (0.2 cm diameter) were randomly divided into 4 groups (*n* = 5-6/group) and the investigator was blinded for treatment allocation. Mice were treated every three days with five i.p. injections of 4-1BB$^{N/C}$EGFR trimerbodies (4 mg/kg), or every week with three i.p. injections of PD-L1 IgG (4 mg/kg), alone or in combination. Mice weights were measured twice a week to monitor toxicity. Mice were euthanized at any sign of distress and/or due to 10-15% of weight loss.

Humanized patient-derived xenograft (PDX) model

For this study, the previously amplified lung PDX TP103 was selected according to its histological type, genetic background (*EGFR* and *TP53* mutated), and huEGFR cell surface expression (26). Tumors were cut into ≈50-mm^3 pieces, and implanted s.c. through a tiny incision into the dorsal space of anesthetized 6-week-old NSG female mice. Tumor growth was monitored by caliper measurements every 3-4 days, and when tumors reached approximately 0.5 cm in diameter, mice were randomized into groups (n = 6-7/group) with similar mean tumor sizes and SDs, and freshly isolated huPBMCs (1 x 10^7 cells/mouse) from healthy donors were i.p. infused. Mice were treated every three days with five i.p. injections of 4-1BB$^{N/C}$EGFR (4 mg/kg). Mice weights were measured once a week to monitor toxicity. Mice were euthanized when the weight loss was≥ 10-15%, when tumor size reached a diameter of 1.0 cm any dimension, when tumors ulcerated, or at any sign of mouse distress.

Statistical analysis

Statistical analysis was performed using GraphPad Prism Software version 6.0. In general, the *in vitro* experiments were done in triplicates and values are presented as mean±SD from one of at least 3 separate experiments. Significant differences (*P* value) were discriminated by applying a two-tailed, unpaired Student's *t* test assuming a normal distribution. *P* values are indicated in the corresponding figures for each experiment. EC50 were calculated using a nonlinear regression curve (log Agonist vs normalized response-variable response). Mean tumor volume are presented for each group using a scatter plot as mean ± SD. To assess the differences between treatment

groups, *P* values were determined by one-way analysis of variance (ANOVA) adjusted by the Bonferroni correction for multiple comparison tests.

RESULTS

Generation and characterization of 4-1BB-agonistic humanized trimerbodies

Anti-hu4-1BB trimerbodies were generated using scFv-encoding genes derived from the anti-hu4-1BB-agonistic SAP3.28 mAb (Fig. S1a), which binds to hu4-1BB CRD-1(27). The SAP3.28 IgG (hereafter referred to as 4-1BB IgG) is a chimeric molecule displaying a humanized V_L domain and a partially humanized V_H domain that preserves the murine FR3 region to retain antigen binding, and the Fc region of murine IgG_1(27). Like urelumab, which recognizes the N-terminus of CRD-1 (28), 4-1BB IgG does not block the hu4-1BB receptor/hu4-1BBL interaction (Fig. S2a-c). Furthermore, we showed that the epitopes of 4-1BB IgG and urelumab do not overlap (Fig. S2d and e).We designed a SAP3.28 scFv-based anti-hu4-1BB N-terminal trimerbody (4-1BB^{N}) by fusing the SAP3.28 scFv to the human collagen XVIII-derived homotrimerization (TIE^{XVIII}) domain by a flexible linker (Fig. S1b and c), and a bispecific trimerbody by fusing the anti-EGFR EGa1 V_{HH} antibody (25) to the C-terminus of the 4-1BB^{N} to generate the construct called 4-1BB$^{N/C}$EGFR (Fig. 1a). Both trimerbodies were purified from conditioned medium from stably transfected HEK293 cells by Strep-Tactin affinity chromatography, with proteins yields (3.5 mg/L and 4.5 mg/L, respectively) that were > 95% pure (Fig. S3a). Mass spectrometry (using MALDI-TOF, not shown) confirmed the absence of the signal sequences in the purified antibodies. SEC-MALS experiments on both 4-1BB^{N} and 4-1BB$^{N/C}$EGFR yielded major peaks with molar masses of 111 and 160 kDa, respectively (Fig. S3b and c), which are consistent with trimeric molecules. Minor peaks at smaller volumes with molar masses of 217 and 340 kDa indicate the presence of dimers of trimers, as previously observed for other trimerbodies (15). Circular dicroism measurements show predominant b-sheet structures and cooperative thermal denaturations ($T_m \approx$ 60 ºC; Fig. S3d and e). Small angle X-ray scattering (SAXS) was used to study the three-dimensional structure of both trimerbodies. The 4-1BB^{N} trimerbody shows a flat distribution, with a well-defined TIE^{XVIII} core in the center and the scFvs partially extended on the same plane, like the spokes on a wheel (Fig. S4 and S5; Table S4) The 4-1BB$^{N/C}$EGFR trimerbody maintains the same planar configuration of 4-1BB^{N} with its additional small-sized

EGFR V_{HH} domains interspersed between the 4-1BB scFvs to resemble a six-bladed ninja star (Fig. 1b; Fig. S5; Table S4).

Biolayer interferometry (BLI) was used to measure the association and dissociation kinetics of 4-1BB^{N} and 4-1BB$^{N/C}$EGFR binding to hu4-1BB, and of 4-1BB$^{N/C}$EGFR and the anti-EGFR ATTACK antibody (29) binding to huEGFR (Fig. 1c). The bispecific ATTACK antibody is an evolution of the tandem trimerbody format (30) which combines three EGFR-binding V_{HH} antibodies with a single CD3-binding scFv (29). All interactions were of high affinity (with low picomolar K_D values), indicating functional trivalence of the trimerbodies towards the antigens displayed on a biosensor surface (Table S5). The kinetics of huEGFR binding by these trivalent antibodies is consistent with previous studies (15, 29). In a complementary experiment, 4-1BB^{N} and the 4-1BB$^{N/C}$EGFR were first loaded onto hu4-1BB immobilized on the surface of biosensors, which were then transferred into buffer containing huEGFR. 4-1BB$^{N/C}$EGFR, but not 4-1BB^{N}, was able to bind soluble huEGFR while remaining bound to the immobilized hu4-1BB, further confirming its bivalence and its capability to bind both antigens simultaneously (Fig. 1d). Furthermore, 4-1BB$^{N/C}$EGFR bound to mouse (mo-), cynomolgus (cy-) and huEGFR (Fig. S6a), as well as to cy4-1BB and hu4-1BB, but to a much lower extent to mo4-1BB (Fig. S6b). Their ability to detect hu4-1BB and huEGFR in a cellular context was analyzed by flow cytometry. The 4-1BB$^{N/C}$EGFR trimerbody bound to wild-type HEK293 (EGFR^{+}) cells, to HEK293 cells transfected to express hu4-1BB on their cell surface (HEK293$^{hu4\text{-}1BB}$), and to mouse 3T3 cells expressing huEGFR (3T3^{huEGFR}) but not to wild-type 3T3 cells (Fig. S7). In contrast, the 4-1BB IgG only bound HEK293$^{hu4\text{-}1BB}$ cells (Fig. S7). To further assess the multivalent binding of 4-1BB$^{N/C}$EGFR, we studied its capacity to inhibit proliferation and EGFR phosphorylation in A431 cells (25). Both 4-1BB$^{N/C}$EGFR and cetuximab, an EGF-competitive inhibitor (31), but neither the anti-human CD20 rituximab nor the parental 4-1BB IgG, inhibited A431 proliferation, in a dose-dependent manner *(P* =0.003 and *P*=0.0005, respectively, for the higher doses of both antibodies, vs. equimolar doses of control antibodies) (Fig. S8a), as well as EGFR phosphorylation (Fig. S8b).

The Fc-free EGFR-targeted 4-1BB-agonistic humanized trimerbody significantly enhances T cell costimulation in the presence of EGFR-expressing cells

The agonist activities of the three SAP3.28-derived antibodies and urelumab were assessed using NF-κB-*luc2*/4-1BB Jurkat cells (Jurkat$^{NF\text{-}\kappa B}$) that constitutively express hu4-1BB on the cell surface and a luciferase reporter driven by a NF-κB response element. Jurkat$^{NF\text{-}\kappa B}$ reporter cells were co-cultured with target cells stably expressing either huFcγRIIb (CHO$^{huFc\gamma RIIb}$) or huEGFR (3T3^{huEGFR}), as well as non-transfected CHO or 3T3 cells as negative controls; the expression of cell surface huFcγRIIb and huEGFR were demonstrated by flow cytometry (Fig. 2a and b). Titrations of bivalent (4-1BB IgG or urelumab), or trivalent (4-1BB^{N} or 4-1BB$^{N/C}$EGFR) anti-hu4-1BB antibodies were then added to the co-cultured cells. In the absence of Fc- or EGFR-mediated antibody crosslinking at the target cell surface (i.e., in co-cultures with non-transfected CHO or 3T3 cells), 4-1BB IgG showed little to no induction over untreated Jurkat$^{NF\text{-}\kappa B}$ cells at all tested concentrations, both anti-hu4-1BB trimerbodies showed an approximately 10-fold induction, and urelumab showed an approximately 20-fold induction (Fig. 2c and d). In the presence of FcγRIIb-mediated crosslinking (i.e., using CHO$^{huFc\gamma RIIb}$ as target cells), 4-1BB IgG induced a NF-κB dose-dependent activation with a 26-fold induction (P = 0.0008)and urelumab's induction was further increased to 40-fold (P = 0.003) (Fig. 2c). Neither trimerbody showed a FcγRIIb-mediated increase in induction (Fig. 2c). The trimerbody-mediated 4-1BB signaling was significantly strengthened when target cells expressed huEGFR(P = 0.0008), leading to a 40-foldincrease of NF-κB luciferase reporter activity (Fig. 2d). Induction by 4-1BB IgG, urelumab, and 4-1BB^{N} was not affected by huEGFR expression (Fig. 2d). The negative control antibodies moIgG1, huIgG4, and CEA^{N}, a trimerbody recognizing CEA, showed no activation (Fig. S9a and b).We then used huPBMCs or T cells from healthy donors to investigate the effect of the anti-hu4-1BB antibodies on IFNγ secretion when co-cultured with irradiated 3T3 or 3T3^{huEGFR}cells, both with and without a suboptimal dose of anti-huCD3 mAb. The 4-1BB$^{N/C}$EGFR trimerbody had a dose-dependent activating effect on IFNγ secretion only when huPBMCs or T cells were co-cultured with EGFR^{+} cells; no induction was observed with EGFR^{-} cells (Fig. 2e and f). Under these conditions, the effect of 4-1BB IgG and CEA^{N} was minimal and independent of EGFR expression (Fig. 2e; Fig. S10). These data show that 4-1BB$^{N/C}$EGFR induces strong, EGFR-dependent T cell costimulation and IFNγ secretion that requires initial signaling through the TCR/CD3 complex (signal 1).Subsequently, huPBMCs were co-cultured with irradiated EGFR^{+}PD-L1^{-} (3T3^{huEGFR})

or EGFR^{+}PD-L1^{+} (MDA-MB-231) cells (Fig. 2g) in the presence of 4-1BB$^{N/C}$EGFR and the PD-L1–blocking antibody atezolizumab. When combined with a suboptimal dose of anti-huCD3 mAb, the 4-1BB$^{N/C}$EGFR trimerbody significantly enhanced IFNγ secretion (P = 0.0007 3T3^{huEGFR} cells; P = 0.0002 MDA-MB-231 cells) (Fig. 2h). The addition of atezolizumab significantly increased IFNγ levels when huPBMCs were co-cultured with MDA-MB-231 cells in the presence of 4-1BB$^{N/C}$EGFR (P = 0.02) (Fig. 2h).

Pharmacokinetics of ^{89}Zr-labeled 4-1BB$^{N/C}$EGFR trimerbody

The 4-1BB$^{N/C}$EGFR trimerbody retained close to 100% of its initial binding activity after 4 days in human serum at 37 °C (Fig. S11 a and b). Chelation with p-SCN-Bn-Deferoxamine (Df) of the 4-1BB$^{N/C}$EGFR trimerbody did not alter its SDS-PAGE migration pattern nor compromise its binding activity (Fig. S12a and b). After radiolabeling, the RCY (radiolabeling yield) and RQP (radiochemical purity) of purified [^{89}Zr]Zr-Df-4-1BB$^{N/C}$EGFR were 40% and 95%, respectively. The AIC values were 10.97 and -22.66 for one and two compartment of [^{89}Zr]Zr-Df-4-1BB$^{N/C}$EGFR respectively, thus, the disposition of the 4-1BB$^{N/C}$EGFR trimerbody was better explained through a bicompartmental model (Table S6). After intravenous administration, the elimination of [^{89}Zr]Zr-Df-4-1BB$^{N/C}$EGFR was biphasic, with a half-time of 7.3 hours for the rapid distribution phase and 66.8 hours for the slow distribution phase (Fig. 3a). The volume of distribution at steady state was 66.5 mL (2.63 L/Kg) and the plasma clearance 0.97 mL/h (37.6 mL/Kg/h). As the blood-to-plasma ratio was 0.62, the blood clearance value obtained was very low (0.062 L/Kg/h) compared with the cardiac output (21.7 L/Kg/h in mouse), which is generally desirable for developing a drug with a low dosage regimen (32).

Anti-tumor activity of the Fc-free EGFR-targeted 4-1BB-agonistic humanized trimerbody

We tested the 4-1BB$^{N/C}$EGFR trimerbody for anti-tumor activity in huPBMC-driven humanized immunoavatar mouse models. Rag2$^{-/-}$ IL2Rγ^{null} mice were intraperitoneally (i.p.) injected with huPBMCs and then human HT-29 CRC cells were subcutaneously (s.c.) inoculated (Fig. 3b). Transferred human T cells become activated and develop pathogenic xeno-reactivity, a process called xenograft-versus-host disease

(xGVHD) (33), which is a valuable model for testing immunomodulatory strategies, where the engrafted human T cells are amenable for modulation by therapeutic agents (34-36). When tumors reached approximately 0.4 cm in diameter mice were treated with five trimerbody (CEA^N or 4-$1BB^{N/C}$EGFR) i.p. injections at 3/4-day intervals, or three weekly equimolar doses of 4-1BB IgG, as depicted in Figure 3b. The dose and treatment schedule was designed in a similar way to what was conducted with the anti-mo4-1BB agonists in an immunocompetent model of CRC (15). The 4-$1BB^{N/C}$EGFR-treated group showed a significantly slower tumor growth compared with the untreated group (P = 0.01), and the CEA^N-treated groups (P = 0.004) (Fig. 3c). Notably, the humanized 4-$1BB^{N/C}$EGFR trimerbody provided anti-tumor activity *in vivo* comparable to the 4-1BB IgG (Fig. 3c).

We next sought to determine whether the anti-tumor effect would also occur in an $EGFR^+$ NSCLC PDX-bearing huPBMC-driven humanized NSG mice model (TP103, Fig. 3d and e). As shown in Figure 3f, the 4-$1BB^{N/C}$EGFR-treated mice showed a reduced tumor growth compared with the control group. The improved tumor growth control was accompanied of significant changes in the TIL infiltration pattern. In both groups, a diffuse infiltration of $CD3^+$ T lymphocytes surrounding and involving tumor cell nests was detected (Fig. S13). In the PBS-treated mice, there was a prevalence of $CD4^+$ T cells with a CD4/CD8 ratio of 2.8 (Fig. 3g-i). In the 4-$1BB^{N/C}$EGFR-treated group, a significant increase in the number of $CD8^+$ T cells (P =0.04) was observed, accompanied by a reduction in the number of $Foxp3^+$ cells (P = 0.01) (Fig. 3g-i; Fig. S13).

We compared the toxicity profile in huPBMC-driven humanized NSG mice treated with 4-1BB IgG or 4-$1BB^{N/C}$EGFR trimerbody (6 mg/kg) once a week for 3 weeks and euthanized 1 week later. The histologic study of the livers revealed that 4-1BB IgG treatment exacerbated xGVHD. Details of the liver infiltration in a representative mouse of each group of treatment are depicted in Figure 3j, showing extensive perivascular mononuclear cell infiltration in the group treated with the IgG-based 4-1BB agonist. We then studied the concentrations of human IFNγ in serum samples collected at sacrifice. 4-1BB IgG treatment significantly increase IFNγ levels over 4-$1BB^{N/C}$EGFR treatment (P = 0.001), where the levels were comparable to PBS-treated animals (Fig. 3k).

The combination of 4-1BB$^{N/C}$EGFR and atezolizumab induces tumor regression

The therapeutic potential of combining 4-1BB$^{N/C}$EGFR with the PD-L1 blocker atezolizumab was investigated in huPBMC-driven humanized NSG mice bearing human EGFR^{+}PD-L1^{+} MDA-MB-231 (Fig. 2g) TNBC xenografts (Fig. 4a). Atezolizumab monotherapy was able to reduce tumor growth by ~60%, while 4-1BB$^{N/C}$EGFR monotherapy showed a ~90% tumor growth reduction (Fig. 4b). The combination of atezolizumab plus 4-1BB$^{N/C}$EGFR resulted in an additional decrease in tumor growth (Fig. 4b). In the PBS-treated group large nests of neoplastic pleomorphic cells with intense cytokeratin (CK) expression with dense lymphocyte infiltration (Fig. 4c and d) were observed. Importantly, the percentage of CK^{+} cells was significantly lower in the 4-1BB$^{N/C}$EGFR monotherapy group (P = 0.04) and in the combination therapy group (P = 0.0002) than in atezolizumab monotherapy group (Fig. 4c). With combination therapy, the percentage of CK^{+} cells was at most 30% in 5 out of 6 mice and in one mouse, TNBC cells were completely eradicated (Fig. 4e). This reduction in tumor burden was associated with a significantly increased proportion of CD8^{+} T cells in the 4-1BB$^{N/C}$EGFR-treated groups (P = 0.03 and P = 0.04) (Fig. 4d and e).

DISCUSSION

Immune checkpoint receptors, both coinhibitory and costimulatory, are membrane molecules expressed by immune cells that regulate the activation and effector functions of T cells (37). These regulatory receptors can be manipulated by the exogenous administration of antibodies to enhance pre-existing anti-tumor immunity (38). The blockade of inhibitory checkpoints, such as CTLA-4 and PD-1/PD-L1, with antagonistic mAbs have shown remarkable efficacy in several types of cancer, with manageable toxicity profiles; however, their overall response rate remains around 30% (39). Agonistic antibodies targeting costimulatory checkpoints, such as 4-1BB, OX40, CD40, GITR, and ICOS, are able to bias T cells towards an effector outcome and overcome anergy-inducing immunosuppressive signaling in the tumor microenvironment, thus providing strong rationale to be combined with ICB (38). However, despite significant interest and effort, no such antibody has yet received regulatory approval. Among them, anti-4-1BB mAbs have shown robust anti-tumor activity in preclinical models (12). However, the clinical development of full-length IgG anti-hu4-1BB-agonistic mAbs is facing serious challenges due to low efficacy (utomilumab) or severe hepatotoxicity (urelumab) (18). We recently generated Fc-free

tumor-targeted murine 4-1BB-agonistic trimerbodies that induced effective anti-tumor immunity without liver toxicity in immunocompetent mice (15).

Here, we characterize a Fc-free bispecific humanized trimerbody which binds to human 4-1BB and EGFR. This 4-1BB$^{N/C}$EGFR trimerbody is efficiently produced and structural studies showed that the trimerbody primarily forms the intended trimeric structure, with protein folding and configuration nearly identical to that of the murine trimerbody (15). The antibody domains are positioned around the human collagen XVIII homotrimerization domain in a hexagonal configuration, and the binding studies provided quantitative evidence for multivalent interactions with both human 4-1BB and EGFR. These results demonstrate the robustness of the trimerbody scaffold to generate functional multivalent and multispecific molecules with a predictable and well-defined structure.

The binding of three TNFRSF receptors to a single trimeric ligand nucleates receptor clustering to induce signaling, but multiple complexes are required for signaling to reach effective levels (40). Anti-4-1BB-agonistic mAbs can be classified as either strong or weak agonists. A strong agonist (e.g. urelumab) can induce signaling activation without FcγR-mediated crosslinking, while a weak agonistic (e.g. utomilumab) requires FcγR-mediated crosslinking in order to meaningfully induce 4-1BB signaling (41). Here, we demonstrate in a hu4-1BB-reporting cell line that a bivalent (IgG) anti-hu4-1BB antibody derived from the SAP3.28 antibody (27)is dependent on the presence of FcγRIIb to induce 4-1BB signaling and can therefore be classified as weak agonists. However, SAP3.28-derived trimerbodies induce partial 4-1BB signaling even without additional crosslinking, which emphasizes the relevance of trimerbody valence and stoichiometry in the context of agonizing a multimerizing receptor. Importantly, in the presence of EGFR-expressing cells, the trimerbody-4-1BB complexes are further crosslinked, resulting in increased agonistic activity that significantly exceeds that achieved by a 4-1BB IgG crosslinked by FcγRIIb-expressing cells, and was similar to that observed with FcγRIIb-cross-linked urelumab.

When the study was conducted on activated huPBMCs or isolated T cells, the 4-1BB$^{N/C}$EGFR trimerbody did not increase IFNγ secretion above the basal levels, at any of the concentrations analyzed, in the absence of EGFR-specific crosslinking. These results demonstrate that, in contrast to the results from the Jurkat cell-based hu4-1BB reporter assay, under near physiological conditions using activated primary T cells the trimerbody-mediated 4-1BB clustering does not provide effective 4-1BB-

costimulation without additional EGFR-mediated crosslinking. This aspect is particularly relevant, as it shows that effective costimulation is not induced, despite saturating binding of the trimerbody to 4-1BB. This has important implications with regard to off-tumor safety issues, as these results indicate that the trimerbody is not capable of inducing 4-1BB costimulation in TAA-negative tissues.

The humanized EGFR-targeted trimeric 4-1BB-agonistic trimerbody exhibits improved serum stability and a circulatory half-life of nearly three days. We hypothesize that strategies aiming to reinvigorate pre-existing tumor-specific exhausted T cells (42) could benefit from an intermittent boosting strategy, to reduce systemic exposure and potential toxicity. This may be especially important when using a relatively ubiquitous TAA, such as EGFR, for targeted 4-1BB costimulation. The relatively short half-life combined with the TAA-targeted approach would allow the selective accumulation of the 4-1BB$^{N/C}$EGFR trimerbody in the tumor area and in tumor cell–infiltrated lymph nodes. In fact, it has been shown that EGFR expression is related with lymph node involvement and tumor grade in CRC. Also, lymph node-involved CRCs showed higher scores of EGFR staining than control groups (43).

We have recently shown that treatment of immunocompetent transgenic mice expressing huEGFR in the liver (ΔEGFR-tg) (44) with IgG-based anti-mouse 4-1BB agonist resulted in nonspecific immune stimulation and hepatotoxicity (22). In contrast, none of these features were observed in ΔEGFR-tg mice treated with the Fc-free EGFR-specific anti-mouse 4-1BB-agonistic 1D8$^{N/C}$EGa1 trimerbody (22),despite the fact that the anti-EGFR EGa1 V_{HH} recognize huEGFR and moEGFR. These results further validate the safety profile of Fc-free trimerbodies in systemic cancer immunotherapy protocols. Here, we demonstrated that treatment of huPBMC-driven immunoavatar mice (36)with the anti-4-1BB-agonistic IgG resulted in enhanced activation of adoptively transferred human T cells and exacerbation of hepatic xGVHD. In contrast, treatment with the 4-1BBL$^{N/C}$EGFR trimerbody induced human IFNγ serum levels and liver infiltration similar to that observed in PBS-treated animals.

Despite the limitations of current mouse models for the study of human tumors, such as the development of xGVHD , and insufficient engraftment of some human immune subsets (45), we demonstrated that in in huPBMC humanized immunoavatar mouse models of human CRC and TNBC, 4-1BB$^{N/C}$EGFR monotherapy provided significant anti-tumor activity. This effect was confirmed in a humanized PDX model of

human NSCLC where treatment with 4-1BB$^{N/C}$EGFR showed a significant reduction in tumor growth, which was associated with a significant increase in the percentage of $CD8^+$ TIL and a substantial improvement of the $CD8^+$ T cell/Treg ratio, from 7.5 in the control-treated mice to 50 in the 4-1BB$^{N/C}$EGFR-treated mice. EGFR can be an effective target for the development of a broadly applicable tumor-specific 4-1BB mediated immunotherapy. In most solid tumors (including lung, colorectal, prostate, pancreatic, head and neck, liver, renal, urothelial and endometrial cancers, along with glioblastoma) more than 50% of patients display a moderate to strong expression of EGFR (46). Furthermore, in humanized mice bearing aggressive $EGFR^+$ TNBC CLDX expressing high-levels of PD-L1, the combination of 4-1BB$^{N/C}$EGFR with atezolizumab further improved anti-tumor activity, resulting in 1 out of 6 mice undergoing complete regression.

The primary anti-tumor mechanism of anti-4-1BB IgG_1 mAbs is the activation of $CD8^+$ T cells after co-engagement of the inhibitory FcγRIIb receptor (47). However, FcγRIIb interactions in the liver are responsible for the liver toxicity of anti-4-1BB IgG_{2a} mAbs (48-50), which primarily act by depleting Treg cells through interactions with activating FcγR receptors (47). However, these activating FcγR interactions and the subsequent FcγR-mediated depletion of 4-1BB$^+$cells may compromise anti-tumor immunity (41). These findings outline a very intricate scenario in which the number of $CD8^+$ TILs, Treg cells, and $Fc\gamma R^+$ cells, along with the relative abundances of activating and inhibitory FcγRs, are likely to determine patient outcomes and must be considered before deciding whether full-length IgG anti-4-1BB agonists are indicated (51). An additional consideration is the competition between administered therapeutic mAbs and endogenous immunoglobulins for FcγRs, which will affect the Fc receptor binding of anti-4-1BB agonists and thereby affect their mechanism of action (51). Recently, several IgG-based tumor–targeted 4-1BB agonists have been engineered with effector-silent Fc regions that retain FcRn-driven half-life extension while reducing binding to FcγRs (52, 53), indicating that it can be desirable for a therapeutic antibody to avoid these interactions. However, these mutations may affect mAb stability, and introduce potentially immunogenic sites (54). The trimerbody described in this study has no Fc region and thereby ensures completely FcγR-independent 4-1BB clustering and crosslinking, avoiding residual binding activities shown in “silenced” Fc regions (55), and may be more easily systematized and applied in a clinical setting.

Here, we show that the combination of a humanized tumor-specific Fc-free 4-1BB-agonistic trimerbody with an immune checkpoint blocker mAb resulted in a greater therapeutic index compared to either monotherapy. These results demonstrate the benefits of combination therapies using both costimulatory and ICB immunotherapy strategies, and the suitability of the trimerbody platform for enacting costimulatory strategies with high efficacy while avoiding adverse reactions mediated by the Fc region.

Acknowledgements: We thank M. Glennie and A. Villalobos for reagents, and Diamond Light Source (UK) for provision of synchrotron radiation at beamline B21.

Reference List

1. Mahoney KM, Rennert PD, Freeman GJ. Combination cancer immunotherapy and new immunomodulatory targets. Nat Rev Drug Discov 2015;14:561-84.
2. Chamoto K, Hatae R, Honjo T. Current issues and perspectives in PD-1 blockade cancer immunotherapy. Int J Clin Oncol 2020;25:790-800.
3. Wei SC, Duffy CR, Allison JP. Fundamental Mechanisms of Immune Checkpoint Blockade Therapy. Cancer Discov 2018;8:1069-86.
4. Melero I, Hervas-Stubbs S, Glennie M, Pardoll DM, Chen L. Immunostimulatory monoclonal antibodies for cancer therapy. Nat Rev Cancer 2007;7:95-106.
5. Kwon BS, Weissman SM. cDNA sequences of two inducible T-cell genes. Proc Natl Acad Sci U S A 1989;86:1963-7.
6. Saoulli K, Lee SY, Cannons JL, Yeh WC, Santana A, Goldstein MD, et al. CD28-independent, TRAF2-dependent costimulation of resting T cells by 4-1BB ligand. J Exp Med 1998;187:1849-62.
7. Shuford WW, Klussman K, Tritchler DD, Loo DT, Chalupny J, Siadak AW, et al. 4-1BB costimulatory signals preferentially induce CD8+ T cell proliferation and lead to the amplification in vivo of cytotoxic T cell responses. J Exp Med 1997;186:47-55.
8. Wilcox RA, Tamada K, Flies DB, Zhu G, Chapoval AI, Blazar BR, et al. Ligation of CD137 receptor prevents and reverses established anergy of CD8+ cytolytic T lymphocytes in vivo. Blood 2004;103:177-84.
9. Kroon HM, Li Q, Teitz-Tennenbaum S, Whitfield JR, Noone AM, Chang AE. 4-1BB costimulation of effector T cells for adoptive immunotherapy of cancer: involvement of Bcl gene family members. J Immunother 2007;30:406-16.

10. Sabbagh L, Pulle G, Liu Y, Tsitsikov EN, Watts TH. ERK-dependent Bim modulation downstream of the 4-1BB-TRAF1 signaling axis is a critical mediator of CD8 T cell survival in vivo. J Immunol 2008;180:8093-101.
11. Melero I, Hirschhorn-Cymerman D, Morales-Kastresana A, Sanmamed MF, Wolchok JD. Agonist antibodies to TNFR molecules that costimulate T and NK cells. Clin Cancer Res 2013;19:1044-53.
12. Melero I, Shuford WW, Newby SA, Aruffo A, Ledbetter JA, Hellstrom KE, et al. Monoclonal antibodies against the 4-1BB T-cell activation molecule eradicate established tumors. Nat Med 1997;3:682-5.
13. Taraban VY, Rowley TF, O'Brien L, Chan HT, Haswell LE, Green MH, et al. Expression and costimulatory effects of the TNF receptor superfamily members CD134 (OX40) and CD137 (4-1BB), and their role in the generation of anti-tumor immune responses. Eur J Immunol 2002;32:3617-27.
14. Wilcox RA, Flies DB, Zhu G, Johnson AJ, Tamada K, Chapoval AI, et al. Provision of antigen and CD137 signaling breaks immunological ignorance, promoting regression of poorly immunogenic tumors. J Clin Invest 2002;109:651-9.
15. Compte M, Harwood SL, Munoz IG, Navarro R, Zonca M, Perez-Chacon G, et al. A tumor-targeted trimeric 4-1BB-agonistic antibody induces potent anti-tumor immunity without systemic toxicity. Nat Commun 2018;9:4809.
16. Li F, Ravetch JV. Antitumor activities of agonistic anti-TNFR antibodies require differential FcgammaRIIB coengagement in vivo. Proc Natl Acad Sci U S A 2013;110:19501-6.
17. Xu Y, Szalai AJ, Zhou T, Zinn KR, Chaudhuri TR, Li X, et al. Fc gamma Rs modulate cytotoxicity of anti-Fas antibodies: implications for agonistic antibody-based therapeutics. J Immunol 2003;171:562-8.
18. Ascierto PA, Simeone E, Sznol M, Fu YX, Melero I. Clinical experiences with anti-CD137 and anti-PD1 therapeutic antibodies. Semin Oncol 2010;37:508-16.
19. Segal NH, Logan TF, Hodi FS, McDermott D, Melero I, Hamid O, et al. Results from an Integrated Safety Analysis of Urelumab, an Agonist Anti-CD137 Monoclonal Antibody. Clin Cancer Res 2017;23:1929-36.
20. Chester C, Sanmamed MF, Wang J, Melero I. Immunotherapy targeting 4-1BB: mechanistic rationale, clinical results, and future strategies. Blood 2018;131:49-57.

662 21. Mikkelsen K, Harwood SL, Compte M, Merino N, Molgaard K, Lykkemark S, et al.
663 Carcinoembryonic Antigen (CEA)-Specific 4-1BB-Costimulation Induced by CEA-
664 Targeted 4-1BB-Agonistic Trimerbodies. Front Immunol 2019;10:1791.
665 22. Compte M, Harwood SL, Martinez-Torrecuadrada J, Perez-Chacon G, Gonzalez-
666 Garcia P, Tapia-Galisteo A, et al. Case Report: An EGFR-Targeted 4-1BB-agonistic
667 Trimerbody Does Not Induce Hepatotoxicity in Transgenic Mice With Liver Expression
668 of Human EGFR. Front Immunol 2020;11:614363.
669 23. Estrada C, Gomez C, Martin C, Moncada S, Gonzalez C. Nitric oxide mediates
670 tumor necrosis factor-alpha cytotoxicity in endothelial cells. Biochem Biophys Res
671 Commun 1992;186:475-82.
672 24. Cuesta AM, Sanchez-Martin D, Sanz L, Bonet J, Compte M, Kremer L, et al. In
673 vivo tumor targeting and imaging with engineered trivalent antibody fragments
674 containing collagen-derived sequences. PLoS One 2009;4:e5381.
675 25. Schmitz KR, Bagchi A, Roovers RC, Van Bergen En Henegouwen PM, Ferguson
676 KM. Structural evaluation of EGFR inhibition mechanisms for nanobodies/VHH
677 domains. Structure 2013;21:1214-24.
678 26. Quintanal-Villalonga A, Molina-Pinelo S, Cirauqui C, Ojeda-Marquez L, Marrugal
679 A, Suarez R, et al. FGFR1 Cooperates with EGFR in Lung Cancer Oncogenesis, and
680 Their Combined Inhibition Shows Improved Efficacy. J Thorac Oncol 2019;14:641-55.
681 27. Al-Shamkhani A, Chan HTC, Cragg MS, French RR, Glennie M, Wolchok JD, et
682 al. Immunomodulatory antibodies 2017;PCT/EP2016/076747
683 28. Chin SM, Kimberlin CR, Roe-Zurz Z, Zhang P, Xu A, Liao-Chan S, et al. Structure
684 of the 4-1BB/4-1BBL complex and distinct binding and functional properties of
685 utomilumab and urelumab. Nat Commun 2018;9:4679.
686 29. Harwood SL, Álvarez-Cienfuegos A, Nunez-Prado N, Compte M, Hernandez-Perez
687 S, Merino N, et al. ATTACK, a novel bispecific T cell-recruiting antibody with trivalent
688 EGFR binding and monovalent CD3 binding for cancer immunotherapy.
689 Oncoimmunology 2017;7:e1377874.
690 30. Alvarez-Cienfuegos A, Nunez-Prado N, Compte M, Cuesta AM, Blanco-Toribio A,
691 Harwood SL, et al. Intramolecular trimerization, a novel strategy for making
692 multispecific antibodies with controlled orientation of the antigen binding domains. Sci
693 Rep 2016;6:28643.

694 31. Li S, Schmitz KR, Jeffrey PD, Wiltzius JJ, Kussie P, Ferguson KM. Structural basis
695 for inhibition of the epidermal growth factor receptor by cetuximab. Cancer Cell
696 2005;7:301-11.
697 32. Toutain PL, Bousquet-Melou A. Bioavailability and its assessment. J Vet Pharmacol
698 Ther 2004;27:455-66.
699 33. Nervi B, Rettig MP, Ritchey JK, Wang HL, Bauer G, Walker J, et al. Factors
700 affecting human T cell engraftment, trafficking, and associated xenogeneic graft-vs-host
701 disease in NOD/SCID beta2mnull mice. Exp Hematol 2007;35:1823-38.
702 34. Carroll RG, Carpenito C, Shan X, net-Desnoyers G, Liu R, Jiang S, et al. Distinct
703 effects of IL-18 on the engraftment and function of human effector CD8 T cells and
704 regulatory T cells. PLoS One 2008;3:e3289.
705 35. Mutis T, van Rijn RS, Simonetti ER, arts-Riemens T, Emmelot ME, van BL, et al.
706 Human regulatory T cells control xenogeneic graft-versus-host disease induced by
707 autologous T cells in RAG2-/-gammac-/- immunodeficient mice. Clin Cancer Res
708 2006;12:5520-5.
709 36. Sanmamed MF, Rodriguez I, Schalper KA, Onate C, Azpilikueta A, Rodriguez-
710 Ruiz ME, et al. Nivolumab and Urelumab Enhance Antitumor Activity of Human T
711 Lymphocytes Engrafted in Rag2-/-IL2Rgammanull Immunodeficient Mice. Cancer Res
712 2015;75:3466-78.
713 37. Chen L, Flies DB. Molecular mechanisms of T cell co-stimulation and co-inhibition.
714 Nat Rev Immunol 2013;13:227-42.
715 38. Melero I, Berman DM, Aznar MA, Korman AJ, Perez Gracia JL, Haanen J.
716 Evolving synergistic combinations of targeted immunotherapies to combat cancer. Nat
717 Rev Cancer 2015;15:457-72.
718 39. Baumeister SH, Freeman GJ, Dranoff G, Sharpe AH. Coinhibitory Pathways in
719 Immunotherapy for Cancer. Annu Rev Immunol 2016;34:539-73.
720 40. Wajant H. Principles of antibody-mediated TNF receptor activation. Cell Death
721 Differ 2015;22:1727-41.
722 41. Qi X, Li F, Wu Y, Cheng C, Han P, Wang J, et al. Optimization of 4-1BB antibody
723 for cancer immunotherapy by balancing agonistic strength with FcgammaR affinity. Nat
724 Commun 2019;10:2141.
725 42. Menk AV, Scharping NE, Rivadeneira DB, Calderon MJ, Watson MJ, Dunstane D,
726 et al. 4-1BB costimulation induces T cell mitochondrial function and biogenesis
727 enabling cancer immunotherapeutic responses. J Exp Med 2018;215:1091-100.

728 43. Mokhtari M, Ardestani MM, Movahedipour M. An immunohistochemical study of
729 EGFR expression in colorectal cancer and its correlation with lymph nodes status and
730 tumor grade. J Res Med Sci 2012;17:741-4.
731 44. Lopez-Luque J, Caballero-Diaz D, Martinez-Palacian A, Roncero C, Moreno-
732 Caceres J, Garcia-Bravo M, et al. Dissecting the role of epidermal growth factor
733 receptor catalytic activity during liver regeneration and hepatocarcinogenesis.
734 Hepatology 2016;63:604-19.
735 45. Morillon YM, Sabzevari A, Schlom J, Greiner JW. The Development of Next-
736 generation PBMC Humanized Mice for Preclinical Investigation of Cancer
737 Immunotherapeutic Agents. Anticancer Res 2020;40:5329-41.
738 46. The Human Protein Atlas; EGFR https://www proteinatlas org/ENSG00000146648-
739 EGFR/pathology 2020
740 47. Buchan SL, Dou L, Remer M, Booth SG, Dunn SN, Lai C, et al. Antibodies to
741 Costimulatory Receptor 4-1BB Enhance Anti-tumor Immunity via T Regulatory Cell
742 Depletion and Promotion of CD8 T Cell Effector Function. Immunity 2018;49:958-70.
743 48. Dubrot J, Milheiro F, Alfaro C, Palazon A, Martinez-Forero I, Perez-Gracia JL, et
744 al. Treatment with anti-CD137 mAbs causes intense accumulations of liver T cells
745 without selective antitumor immunotherapeutic effects in this organ. Cancer Immunol
746 Immunother 2010;59:1223-33.
747 49. Niu L, Strahotin S, Hewes B, Zhang B, Zhang Y, Archer D, et al. Cytokine-
748 mediated disruption of lymphocyte trafficking, hemopoiesis, and induction of
749 lymphopenia, anemia, and thrombocytopenia in anti-CD137-treated mice. J Immunol
750 2007;178:4194-213.
751 50. Vonderheide RH, Glennie MJ. Agonistic CD40 antibodies and cancer therapy. Clin
752 Cancer Res 2013;19:1035-43.
753 51. Álvarez-Vallina L. 4-1BB-mediated cancer immunotherapy: 'mission impossible' for
754 non-engineered IgGs? Precision Cancer Medicine 2019;2:1.
755 52. Claus C, Ferrara C, Xu W, Sam J, Lang S, Uhlenbrock F, et al. Tumor-targeted 4-
756 1BB agonists for combination with T cell bispecific antibodies as off-the-shelf therapy.
757 Sci Transl Med 2019;11
758 53. Hinner MJ, Aiba RSB, Jaquin TJ, Berger S, Durr MC, Schlosser C, et al. Tumor-
759 Localized Costimulatory T-Cell Engagement by the 4-1BB/HER2 Bispecific Antibody-
760 Anticalin Fusion PRS-343. Clin Cancer Res 2019;25:5878-89.

54. Schlothauer T, Herter S, Koller CF, Grau-Richards S, Steinhart V, Spick C, et al. Novel human IgG1 and IgG4 Fc-engineered antibodies with completely abolished immune effector functions. Protein Eng Des Sel 2016;29:457-66.
55. Vafa O, Gilliland GL, Brezski RJ, Strake B, Wilkinson T, Lacy ER, et al. An engineered Fc variant of an IgG eliminates all immune effector functions via structural perturbations. Methods 2014;65:114-26.

Figure Legends

Figure 1. Design and characterization of the humanized Fc-free tumor-targeted 4-1BB-agonistic trimerbody (4-1BB$^{N/C}$EGFR). (a) Schematic diagrams showing the gene layout and domain structure, and arrangement of 4-1BB$^{N/C}$EGFR in solution, as determined by SAXS (b). Rigid-body fitting of the model corresponding to 4-1BB$^{N/C}$EGFR inside the SAXS envelope (colored in pale grey). Each chain has been colored in blue, magenta and cyan. (c) Experimental sensorgrams (black lines) and calculated (red lines) obtained from BLI showing the interactions between 4-1BB^{N} and 4-1BB$^{N/C}$EGFR trimerbodies (at 1 and 5 nM concentrations) and immobilized hu4-1BB (upper panels), and those between anti-huEGFR ATTACK and 4-1BB$^{N/C}$EGFR trimerbody (at 1 and 5 nM concentrations) and immobilized huEGFR (lower panels). The kinetic rate constants used for the calculated curves are given in Table S5. (d) Simultaneous binding to both immobilized hu4-1BB and huEGFR in solution was demonstrated for 4-1BBL$^{N/C}$EGFR (green) but not 4-1BB^{N} (black); 5 nM of either trimerbody first bound to immobilized hu4-1BB, after which the biosensors were moved into 10 nM huEGFR.

Figure 2. The 4-1BB$^{N/C}$EGFR trimerbody significantly enhances *in vitro* T cell costimulation in the presence of huEGFR-expressing cells and signal 1. Flow cytometry analysis of huFcγRIIb (CD32) expression in CHO and CHO$^{huFc\gamma RIIb}$ cells (a), and of huEGFR expression in 3T3 and 3T3^{huEGFR} cells (b). Cells incubated with PE-conjugated isotype control mAb are shown as grey-filled histogram. Fluorescence intensity (abscissa) is plotted against relative cell number (ordinate).The numbers indicate the mean fluorescence intensity (MFI).Jurkat$^{hu4\text{-}1BB}$ cells were co-cultured with CHO or CHO$^{huFc\gamma RIIb}$ cells (c) and 3T3 or 3T3^{huEGFR} cells (d) in the presence of 10-fold increasing concentrations of 4-1BB IgG, urelumab, 4-1BB^{N} or 4-1BB$^{N/C}$EGFR antibodies, and after 6 hours at 37 °C luminescence determined. Data were presented as fold induction relative to the values obtained from unstimulated Jurkat$^{hu4\text{-}1BB}$ cells. Representative dose-concentration curves are presented and expressed as a mean ± SD (n = 3). Significance was determined by unpaired Student's t test. Human PBMCs (e) and T cells (f) (1.5 x 10^5/well) isolated from healthy donors were co-cultured with irradiated 3T3 or 3T3^{huEGFR} cells at an E:T ratio of 5:1. The anti-hu4-1BB agonists antibodies (4-1BB IgG or 4-1BB$^{N/C}$EGFR) and controls were added at ten-fold serial

dilutions in the presence or absence of anti-huCD3 mAb (0.05 µg/ml), and IFNγ secretion was analyzed after 72 hours (mean ± SD, *n* = 3). Significance was determined by unpaired Student's *t* test. (g) Flow cytometry analysis of huEGFR expression (upper panel) or huPD-L1 expression (lower panel) in $3T3^{huEGFR}$ and MDA-MB-231 cells. Cells incubated with PE-conjugated isotype control mAbs are shown as grey-filled histogram. (h) Irradiated $EGFR^{+}PD\text{-}L1^{-}$ cells ($3T3^{huEGFR}$) or $EGFR^{+}PD\text{-}L1^{+}$ cells (MDA-MB-231) (3 x 10^4 cells/well) were co-cultured with huPBMCs at a 5:1 E:T ratio, activated with anti-huCD3 mAb (0.05 µg/ml), in the presence of anti-PD-L1 alone or combined with 4-$1BB^{N/C}$EGFR. Cell-free supernatants were measured for IFNγ after 72 hours by ELISA. Data are presented as mean ± SD (*n* = 3). Significance was calculated by an unpaired Student's *t* test. One representative experiment out of three independent experiments were shown (a and c). If primary cells were used, then at least three different donors were tested.

Figure 3. 4-$1BB^{N/C}$EGFR trimerbody displayed significant tumor growth inhibition in humanized mouse models. (a) Pharmacokinetic profile expressed as % ID/ml in plasma vs. time of ^{89}Zr-4-$1BB^{N/C}$EGFR following i.v. administration. Data are shown as mean ± SD (*n* = 2-6). (b) $Rag2^{-/-}IL2R\gamma^{null}$ mice were inoculated s.c. with HT29 tumor cells and i.p. with freshly-isolated huPBMCs, and when tumors reached approximately 0.4 cm in diameter randomized into groups (*n* = 7-8/group) with similar mean tumor sizes and SDs, and treated with PBS, five i.p. injections of CEA^{N} or 4-$1BB^{N/C}$EGFR trimerbodies (4 mg/kg) or with three i.p. injections of 4-1BB IgG (4 mg/kg). (c) Average tumor volume growth of mice in each group are represented. Data are presented as the mean ± SD. Significance was determined by one-way ANOVA adjusted by the Bonferroni correction for multiple comparison test. (d) Analysis of huEGFR expression by IHC in NSCLC PDX TP103. (e) NSG mice were s.c. inoculated with small fragments of previously amplified TP103 and when tumors reached approximately 0.5 cm in diameter randomized into groups (*n* = 6-7/group) with similar mean tumor sizes and SDs, and freshly isolated huPBMCs i.p. injected. Mice were treated with PBS or 4-$1BB^{N/C}$EGFR. (f) Average tumor volume growth of mice in each group are represented. Data are presented as the mean ± SD. Significance was determined by an unpaired Student's *t* test. In both *in vivo* assays, mice weights were measured once a week to monitor toxicity and animals were euthanized at any sign of

distress and/or due to 10-15% of weight loss. Percentage of $CD4^+$ and $CD8^+$cells (g) or $FoxP3^+$ cells (h) on tissue sections from PBS- and 4-1BB$^{N/C}$EGFR-treated mice (mean ± SD, *n* = 4-5). Significance was calculated by an unpaired Student's *t* test. (i) Representative IHC staining for CD4 and CD8 is shown. Tumors were taken from the experiment shown in (c) at termination. (j) H&E staining in representative tissue sections of liver of mice treated with PBS, 4-1BB IgG, and 4-1BB$^{N/C}$EGFR. Scale bars are shown. (k) Human IFNγ serum levels of mice were studied in week four (mean ± SD, *n* = 4). Significance was calculated by an unpaired Student's *t* test.

Figure 4. Combination of 4-1BB$^{N/C}$EGFR and full-length PD-L1–blocking antibodies induces tumor regression in an humanized MDA-MB-231 TNBC xenograft model. (a) NSG mice were inoculated s.c. with MDA-MB-231 tumor cells and injected i.p. with freshly-isolated huPBMCs, and when tumors reached approximately 0.2 cm in diameter randomized into groups (*n* = 5-6/group), and treated with PBS or 4-1BB$^{N/C}$EGFR or atezolizumab alone or in combination. (b) Average tumor volume growth of mice in each group are represented. Data are presented as the mean ± SD. Mice weights were measured once a week and animals were euthanized at any sign of distress and/or due to 10-15% of weight loss. Significance was determined by one-way ANOVA adjusted by the Bonferroni correction for multiple comparison test. Percentage of cytokeratin $(CK)^+$ cells (c) and CD4/CD8 ratio of tumor-infiltrating lymphocytes (TILs) (d) on tumor sections taken from the experiment shown in (b) at termination. Data are presented as mean ± SD (*n* = 4-6). Significance was calculated by an unpaired Student's *t* test. (e) Representative low magnification images of H&E and immunohistochemically stained samples for cytokeratin, CD4 and CD8 are shown. In the combination therapy group two representative specimens are shown, with partial or complete immune-mediated eradication (IME) of TNBC cells.

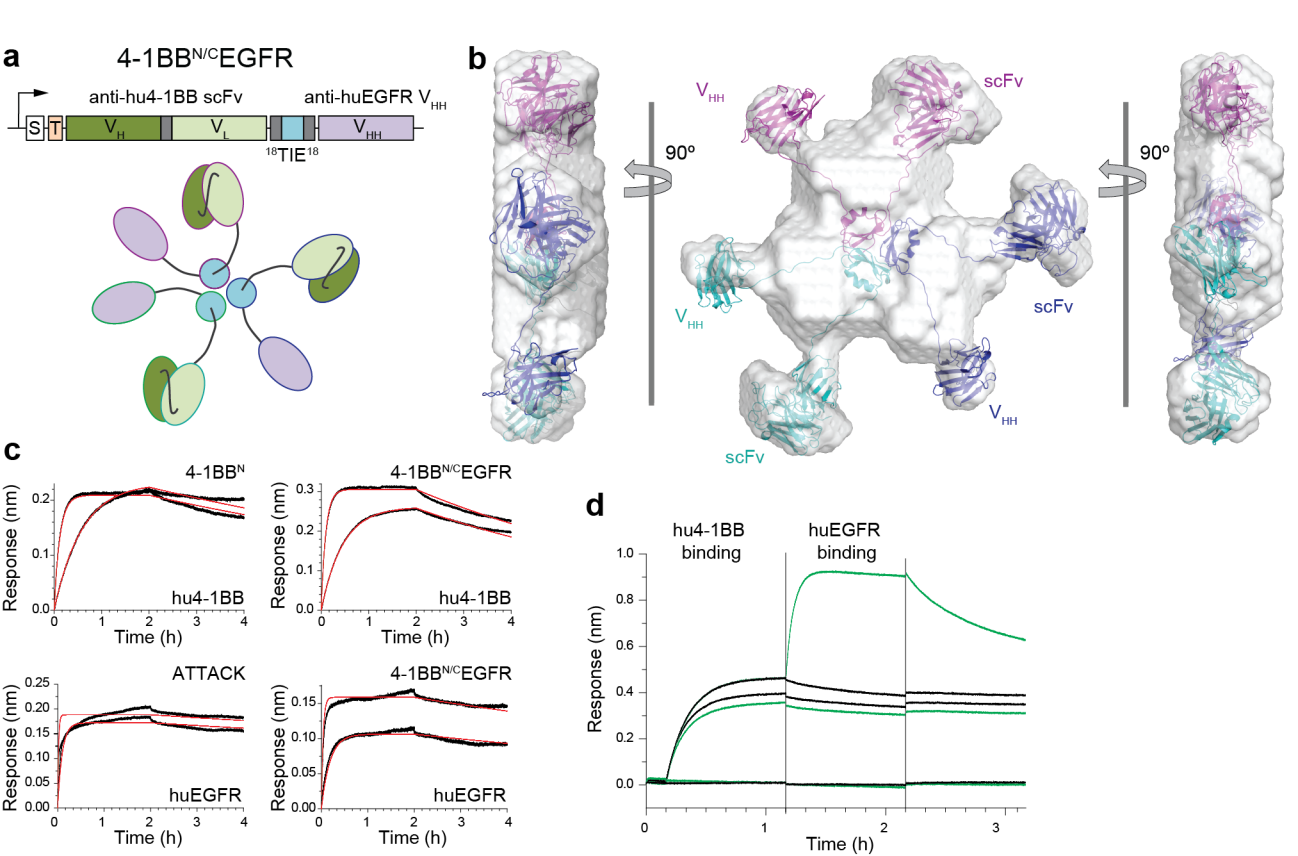
a
4-1BB^N/CEGFR
anti-hu4-1BB scFv
anti-huEGFR V_HH
S
T
V_H
V_L
V_HH
18TIE18
b
V_HH
scFv
90°
V_HH
scFv
V_HH
scFv
90°
c
4-1BB^N
hu4-1BB
4-1BB^N/CEGFR
hu4-1BB
ATTACK
huEGFR
4-1BB^N/CEGFR
huEGFR
Response (nm)
Time (h)
d
hu4-1BB binding
huEGFR binding
Response (nm)
Time (h)

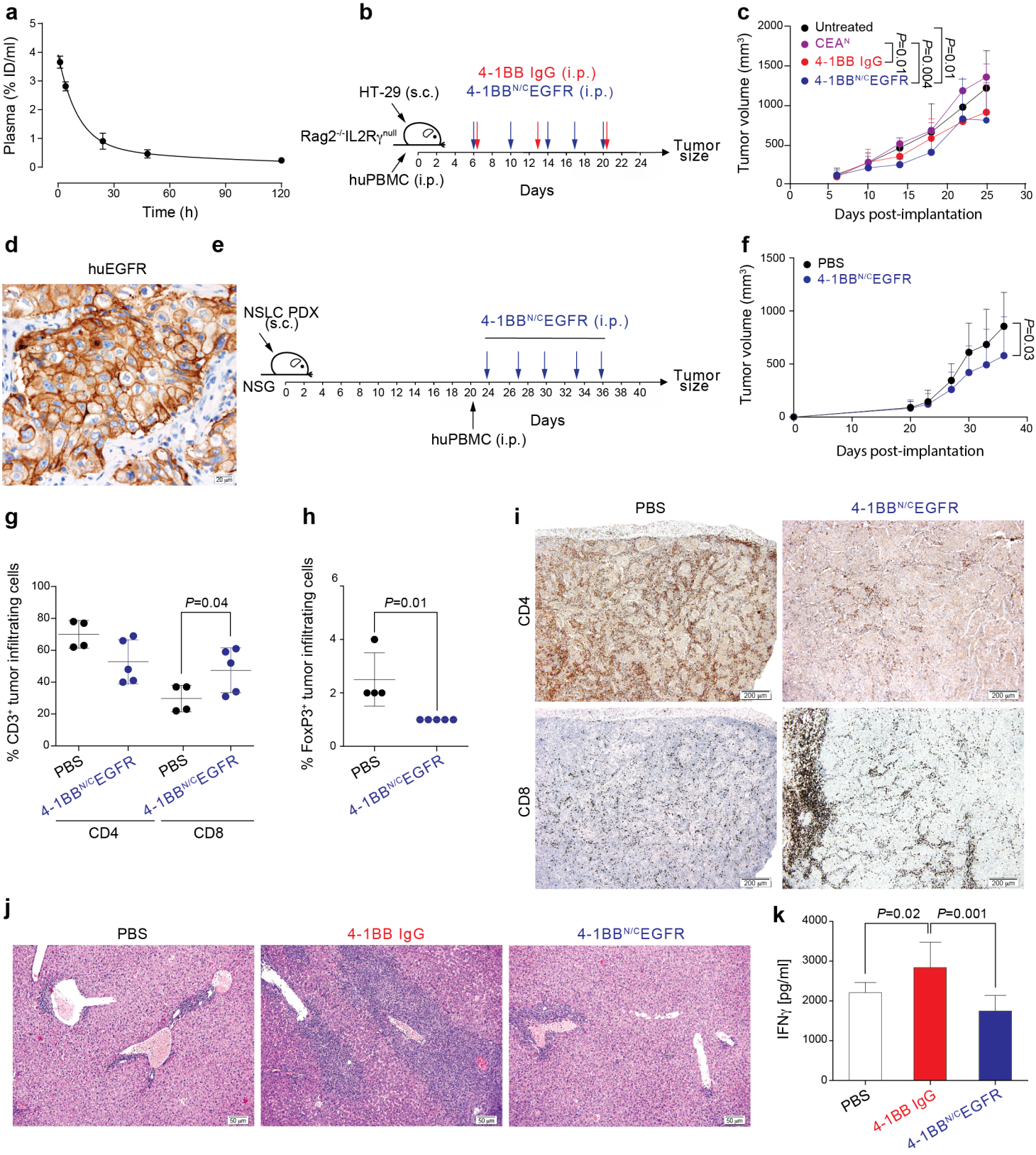
a
Plasma (% ID/ml)
Time (h)
b
4-1BB IgG (i.p.)
4-1BB$^{N/C}$EGFR (i.p.)
HT-29 (s.c.)
Rag2$^{-/-}$IL2Rγ^{null}
huPBMC (i.p.)
Tumor size
Days
c
Untreated
CEA^{N}
4-1BB IgG
4-1BB$^{N/C}$EGFR
P=0.01
P=0.004
P=0.01
Tumor volume (mm^3)
Days post-implantation
d
huEGFR
e
NSLC PDX (s.c.)
NSG
4-1BB$^{N/C}$EGFR (i.p.)
Tumor size
Days
huPBMC (i.p.)
f
PBS
4-1BB$^{N/C}$EGFR
P=0.03
Tumor volume (mm^3)
Days post-implantation
g
% CD3$^+$ tumor infiltrating cells
P=0.04
PBS
4-1BB$^{N/C}$EGFR
PBS
4-1BB$^{N/C}$EGFR
CD4
CD8
h
% FoxP3$^+$ tumor infiltrating cells
P=0.01
PBS
4-1BB$^{N/C}$EGFR
i
PBS
4-1BB$^{N/C}$EGFR
CD4
CD8
j
PBS
4-1BB IgG
4-1BB$^{N/C}$EGFR
k
P=0.02
P=0.001
IFNγ [pg/ml]
PBS
4-1BB IgG
4-1BB$^{N/C}$EGFR

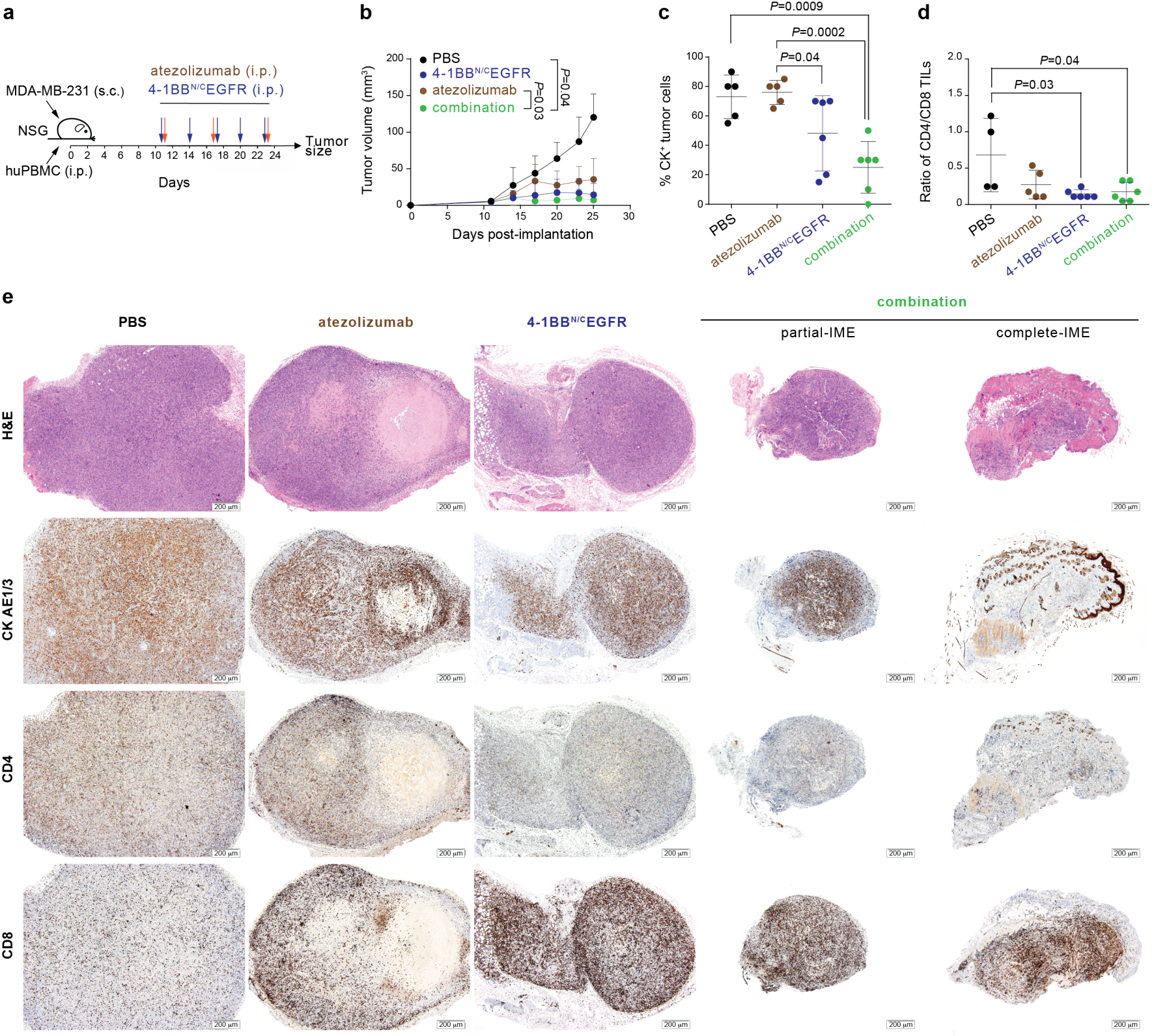
a
atezolizumab (i.p.)
4-1BB$^{N/C}$EGFR (i.p.)
MDA-MB-231 (s.c.)
NSG
huPBMC (i.p.)
0 2 4 6 8 10 12 14 16 18 20 22 24
Days
Tumor size
b
PBS
4-1BB$^{N/C}$EGFR
atezolizumab
combination
P=0.04
P=0.03
Tumor volume (mm^3)
Days post-implantation
c
P=0.0009
P=0.0002
P=0.04
% CK$^+$ tumor cells
PBS
atezolizumab
4-1BB$^{N/C}$EGFR
combination
d
P=0.04
P=0.03
Ratio of CD4/CD8 TILs
PBS
atezolizumab
4-1BB$^{N/C}$EGFR
combination
e
PBS
atezolizumab
4-1BB$^{N/C}$EGFR
combination
partial-IME
complete-IME
H&E
CK AE1/3
CD4
CD8
200 μm

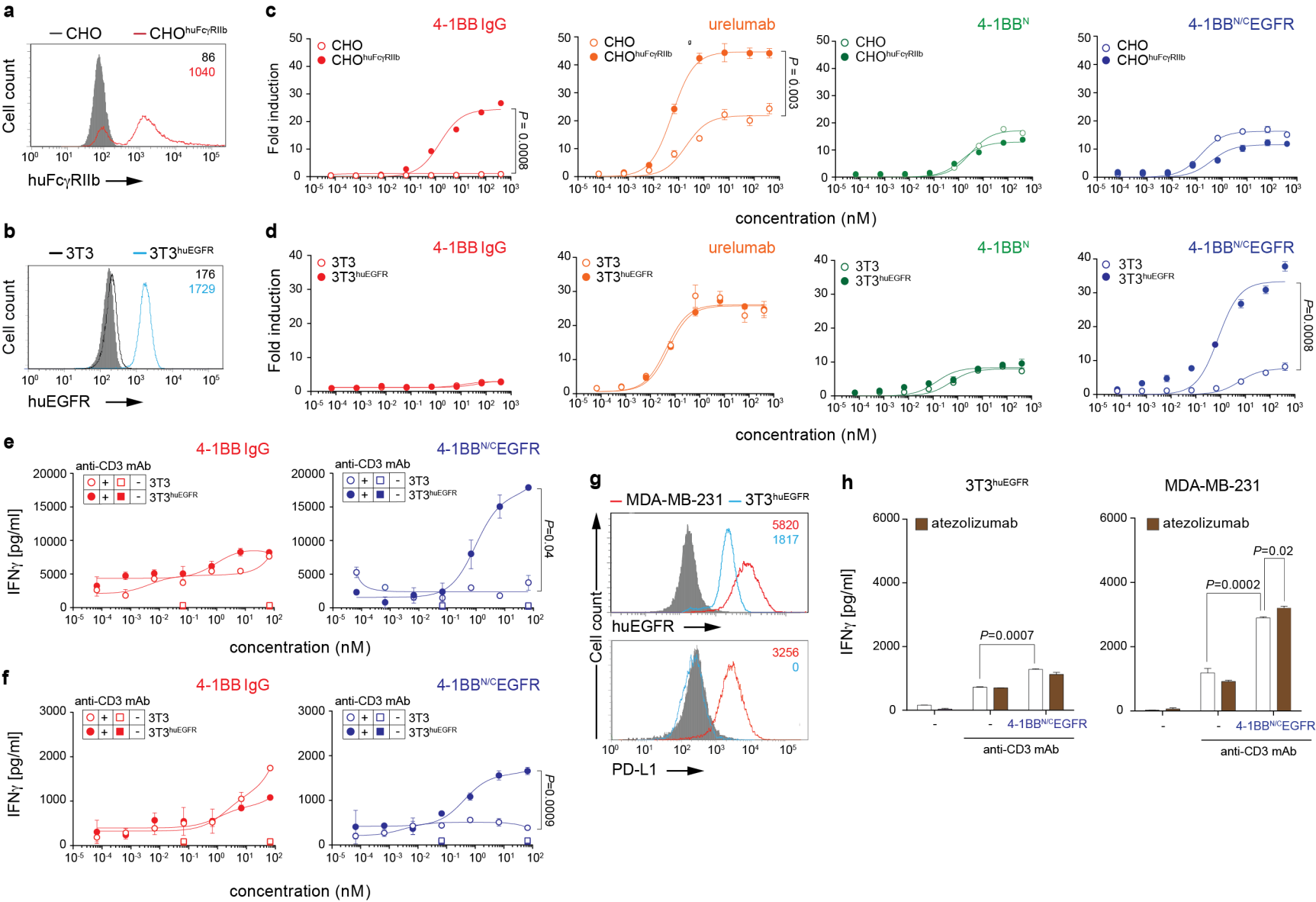
a
CHO
CHO^huFcγRIIb
86
1040
Cell count
huFcγRIIb
b
3T3
3T3^huEGFR
176
1729
Cell count
huEGFR
c
4-1BB IgG
urelumab
4-1BB^N
4-1BB^N/CEGFR
CHO
CHO^huFcγRIIb
Fold induction
P = 0.0008
P = 0.003
concentration (nM)
d
4-1BB IgG
urelumab
4-1BB^N
4-1BB^N/CEGFR
3T3
3T3^huEGFR
Fold induction
P=0.0008
concentration (nM)
e
4-1BB IgG
4-1BB^N/CEGFR
anti-CD3 mAb
3T3
3T3^huEGFR
IFNγ [pg/ml]
P=0.04
concentration (nM)
f
4-1BB IgG
4-1BB^N/CEGFR
anti-CD3 mAb
3T3
3T3^huEGFR
IFNγ [pg/ml]
P=0.0009
concentration (nM)
g
MDA-MB-231
3T3^huEGFR
5820
1817
huEGFR
3256
0
Cell count
PD-L1
h
3T3^huEGFR
MDA-MB-231
atezolizumab
IFNγ [pg/ml]
P=0.0007
P=0.0002
P=0.02
-
4-1BB^N/CEGFR
anti-CD3 mAb